

RESEARCH

Open Access



# Prediction models of breast cancer molecular subtypes based on multimodal ultrasound and clinical features

Hui Li<sup>1†</sup>, Chang-tao Zhang<sup>2†</sup>, Hua-guo Shao<sup>3†</sup>, Lin Pan<sup>4†</sup>, Zhongyun Li<sup>5</sup>, Min Wang<sup>5</sup> and Shi-hao Xu<sup>1\*</sup>

## Abstract

**Background and Aims** Breast cancer classify into four molecular subtypes: Luminal A, Luminal B, HER2-overexpressing (HER2), and triple-negative (TNBC) based on immunohistochemical assessments. The multimodal ultrasound features correlate with biological biomarkers and molecular subtypes, facilitating personalized, precision-guided treatment strategies for patients. In this study, we aimed to explore the differences of multimodal ultrasound features generated from conventional ultrasound (CUS), shear wave elastography (SWE) and contrast-enhanced ultrasound (CEUS) between molecular subtypes of breast cancer, investigate the value of prediction model of breast cancer molecular subtypes based on multimodal ultrasound and clinical features.

**Methods** Breast cancer patients who visited our hospital from January 2023 to June 2024 and underwent CUS, SWE and CEUS were selected, according to inclusion criteria. Based on the selected effective feature subset, binary prediction models of features of CUS, features of SWE, features of CEUS and full parameters were constructed separately for the four breast cancer subtypes Luminal A, Luminal B, HER2, and TNBC, respectively.

**Results** There were ten parameters that showed significant differences between molecular subtypes of breast cancer, including BI-RADS, palpable mass, aspect ratio, maximum diameter, calcification, heterogeneous echogenicity, irregular shape, standard deviation elastic modulus value of lesion, time of appearance, peak intensity. Full parameter models had highest area under the curve (AUC) values in every test set. In aggregate, judging from the values of accuracy, precision, recall, F1 score and AUC, models used features selected from full parameters showed better prediction results than those used features selected from CUS, SWE and CEUS alone (AUC: Luminal A, 0.81; Luminal B, 0.74; HER2, 0.89; TNBC, 0.78).

**Conclusions** In conclusion, multimodal ultrasound features had differences between molecular subtypes of breast cancer and models based on multimodal ultrasound data facilitated the prediction of molecular subtypes.

**Keywords** Multimodal ultrasound, Breast cancer, Molecular subtype, Prediction model

<sup>†</sup>Hui Li, Chang-tao Zhang, Hua-guo Shao and Lin Pan contributed equally to this work.

\*Correspondence:  
Shi-hao Xu  
dcxshvip@wmu.edu.cn

Full list of author information is available at the end of the article



© The Author(s) 2025. **Open Access** This article is licensed under a Creative Commons Attribution-NonCommercial-NoDerivatives 4.0 International License, which permits any non-commercial use, sharing, distribution and reproduction in any medium or format, as long as you give appropriate credit to the original author(s) and the source, provide a link to the Creative Commons licence, and indicate if you modified the licensed material. You do not have permission under this licence to share adapted material derived from this article or parts of it. The images or other third party material in this article are included in the article's Creative Commons licence, unless indicated otherwise in a credit line to the material. If material is not included in the article's Creative Commons licence and your intended use is not permitted by statutory regulation or exceeds the permitted use, you will need to obtain permission directly from the copyright holder. To view a copy of this licence, visit <http://creativecommons.org/licenses/by-nc-nd/4.0/>.

## Introduction

Globally, second only to lung cancer in causing cancer-related fatalities, breast cancer is the most prevalent malignant tumor diagnosed among women [1, 2]. Breast cancer is marked by profound heterogeneity, encompassing diverse genetic signatures, phenotypic expressions, clinical presentations, and responses to therapeutic interventions, making it a complex disease [3, 4]. To address this heterogeneity, a classification system based on immunohistochemical assessments of estrogen receptor (ER), progesterone receptor (PR), human epidermal growth factor receptor 2 (Her-2), and Ki-67 proliferation index, was introduced, segregating breast cancer into four molecular subtypes: Luminal A, Luminal B, HER2-overexpressing (HER2), and triple-negative (TNBC) [5]. This stratification significantly impacts both treatment strategies and patient prognosis [6, 7]. Therefore, accurate identification of these molecular subtypes is crucial for making individualized treatment plans and enhancing patient outcomes.

Ultrasound, renowned for its safety, non-invasiveness, and cost-effectiveness, is routinely employed for breast cancer screening and diagnosis [8]. In the realm of breast cancer diagnosis, conventional ultrasound (CUS) remains a cornerstone examination method [9, 10]. However, contrast-enhanced ultrasound (CEUS) surpasses CUS by concurrently depicting tumor morphology and dynamically elucidating the perfusion patterns within tumor microcirculation, thereby offering supplementary, invaluable insights. Research underscores a correlation between CEUS performance and breast cancer prognostic factors, with the visualized microcirculatory architecture serving as a predictive tool for molecular subtype classification [11, 12]. The shear wave elastography (SWE) image characteristics can visually depict the stiffness distribution and stiffness differences of the lesion, which can then be utilized for the diagnosis of breast tumors. To refine diagnostic precision, multimodal data encompassing B-mode imaging, shear wave elastography assessing tissue stiffness [13], color doppler flow imaging (CDFI) detecting enhanced tumoral blood flow [14], are usually integrated. These multimodal ultrasound-derived features correlate with biological biomarkers and molecular subtypes, facilitating personalized, precision-guided treatment strategies for patients [15, 16].

In this study, we aimed to explore the differences of multimodal ultrasound features generated from CUS, SWE and CEUS between molecular subtypes of breast cancer, investigate the value of prediction model of breast cancer molecular subtypes based on multimodal ultrasound and clinical features.

## Methods

### Patients

Breast cancer patients who visited our hospital from January 2023 to June 2024 were selected. The inclusion criteria were as follows: (1) Surgical resection of the target tumor; (2) Postoperative pathological confirmation of malignancy with complete clinical data; (3) Undergoing CUS, SWE, and CEUS examinations within 2 weeks before surgery; (4) No neoadjuvant chemotherapy or other treatments received before ultrasonography; (5) No history of breast augmentation, pregnancy or lactation. In patients with multiple lesions, only the largest lesion was included and subjected to corresponding pathological analysis. The exclusion criteria were: (1) Patients with surgical contraindications; (2) Any preoperative interventions and treatments, including radiotherapy, chemotherapy or radiofrequency ablation; (3) Patients who had undergone breast prosthesis implantation; (4) Non-standard image acquisition; (5) Contraindications to contrast agents.

### Histopathology and immunohistochemistry

Regarding postoperative pathological findings as the gold standard, all surgical specimens underwent immunohistochemical examination with the diaminobenzidine staining method to obtain the molecular expression levels of ER, PR, Her-2, and Ki-67. The immunohistochemical results were judged by two pathologists separately, and the final decision was determined through joint discussion. The criteria for ER and PR positivity were the presence of brown-yellow granules in the tumor cell nuclei, with the number of positively stained cells  $\geq 1\%$ . For Her-2, positivity was defined as the presence of brown-yellow or yellow granules in the cell membrane and uniform cell membrane staining in  $>10\%$  of cancer cells. The criterion for Ki-67 was that high expression was defined as the presence of brown-yellow granules in the tumor cell nuclei with  $\geq 14\%$  positively stained cells, and low expression as  $<14\%$ . According to the 2017 St. Gallen Breast Cancer Consensus [17], based on the differences in the expression levels of immunohistochemical markers ER, PR, Her-2, and Ki-67, the molecular subtypes were classified as follows: (1) Luminal A, ER (+) and/or PR (+), Her-2 (-), Ki-67 expression  $<14\%$ ; (2) Luminal B, further divided into Her-2 (-) [ER (+) and/or PR (+), Her-2 (-), Ki-67 expression  $\geq 14\%$ ] and Her-2 positive [ER (+) and/or PR (+), Her-2 (+)]; (3) HER2, ER (-), PR (-), Her-2 (+); (4) TNBC, ER (-), PR (-) and Her-2 (-).

### Conventional ultrasound

Using the Mindray Resona 8PRO color doppler ultrasound diagnostic instrument equipped with a superficial probe L14-5WU, patients were instructed to lie supine with their upper arms raised to fully expose both breasts.

After determining the location of the lesion, a physician with over 10 years of experience in breast ultrasound diagnosis performed multi-angle and multi-section scans and stored complete ultrasound image information. Conventional ultrasound documentation included breast mass sonographic features such as lesion location, distance to nipple, size, margins, shape, echogenicity, posterior acoustic features, ductal extension and presence of microcalcifications. The CDFI mode was activated to assess the blood flow characteristics of breast masses according to the Alder grading system: grade 0, no blood flow detected; grade 1, minimal blood flow with 1–2 punctate or short rod-like vessels visible; grade 2, moderate blood flow with 3–4 punctate vessels or one clearly defined vessel visible; grade 3, abundant blood flow with more than 4 punctate vessels or more than two clearly defined vessels visible [18]. Additionally, the masses were classified based on the Breast Imaging Reporting and Data System (BI-RADS) [19].

#### **Shear wave elastography**

Switched to the SWE mode with an elasticity measurement range of 0–140 kPa. Placed the sampling box over the entire lesion and its surrounding normal tissue, froze the image once it stabilized, observe whether there is a hard edge sign around the lesion (i.e., the area surrounding the lesion was red or orange), and evaluated using the SWE 5-type classification: Type I, both the interior and periphery of the lesion appear uniformly dark blue; Type II, light blue or green appears within or around the lesion; Type III, local areas around the lesion appear red or orange, with a relatively uniform blue interior; Type IV, red or orange appears within the lesion, with uneven color distribution; Type V, a ring-shaped distribution of red or orange appears around the lesion, with a relatively uniform blue interior or color loss.

Upon initiation of the SWE mode, the largest portion of the lesion was placed at the center of the sampling box. In cases where the lesion is substantial, the cross-section should be appropriately adjusted to ensure that the margin of the mass is at least 3 mm from the sampling frame. Instruct the patient to hold their breath and select the SWE quality-velocity dual-dynamic mode, applying appropriate pressure until the image within the sampling frame displays a uniform green background devoid of significant purple artifacts, achieving a confidence index of 95–100%, which indicates superior image quality. Then, switch to the grayscale SWE velocity dual mode, where red denotes hard tissue and blue signifies soft tissue. If a uniform green background cannot be achieved, the confidence index will fall below 95%, and the measurement will be excluded from the study.

During SWE measurement, the sampling box is positioned over the entire lesion and the adjacent normal

tissue, encompassing a minimum of 3 mm of the peripheral tissue. Due to the absence of a three-dimensional probe on the instrument, three-dimensional reconstruction of the tumor is not feasible; hence, the relatively accurate method of manual delineation is employed, with the maximum cross-sectional area of the tumor serving as the subject of study.

Manually outlined the tumor, and the system automatically calculated various elastography parameters for the lesion, peripheral area and the area encompassing both the lesion and peripheral area, including the mean elastic modulus ( $E_{mean}$ ), maximum elastic modulus ( $E_{max}$ ), minimum elastic modulus ( $E_{min}$ ), and elastic modulus standard deviation ( $E_{sd}$ ) of the lesion, the mean elastic modulus ( $E_{smean}$ ), maximum elastic modulus ( $E_{smax}$ ), minimum elastic modulus ( $E_{smin}$ ), and elastic modulus standard deviation ( $E_{ssd}$ ) of peripheral area 2 mm around the lesion, the minimum elastic modulus ( $E_{lsmin}$ ), maximum elastic modulus ( $E_{lsmax}$ ), minimum elastic modulus ( $E_{lsmin}$ ), and the elastic modulus standard deviation ( $E_{lssd}$ ) of the area encompassing both the lesion and peripheral area.

#### **Contrast-enhanced ultrasound**

For the contrast-enhanced examination, the vascular probe L9-3U was utilized. The most irregular or hyper-vascular section was selected, and the probe was fixed. The instrument was adjusted to the contrast mode. The contrast agent used was SonoVue (provided by Bracco Suisse SA), a lyophilized powder of sulfur hexafluoride encapsulated in phospholipids, which was reconstituted with 5 mL of normal saline (0.9% NaCl) before use by shaking to form a suspension. A bolus injection of 4.8 mL of the suspension was rapidly administered through the elbow vein, followed by a 5 mL saline flush. Patients were instructed to lie flat and maintain steady breathing. Depending on the number and location of the lesions, one or two injections were administered. Timing commenced at the moment of contrast agent injection, and real-time dynamic observation of contrast agent infusion and washout in the lesions was performed. Continuous observation lasted for 3 min, during which dynamic images were captured and stored. The images were reviewed, and a breast imaging physician with extensive diagnostic experience was assigned to analyze the images, observing the enhancement intensity, enhancement velocity, enhancement distribution, enhancement pattern, presence of perfusion defects, enhancement border, enhancement shape, presence of crab-claw-like pattern, and any changes in enhancement area compared to the 2D image.

Quantitative contrast analysis software was used to generate a time-intensity curve, from which the following parameters were recorded: arrival time of the contrast

agent, time to peak (TTP), ascending slope (AS), peak intensity (PI), base intensity (BI), arrival time (AT), 1/2 descending time (DT/2), descending slope (DS), area under the time-intensity curve (AUTIC), and mean transit time (MTT).

### Statistical analysis

Quantitative data within characteristics of patients were described as the median and quartile. Categorical data were described as count and constituent ratio. Comparisons between groups of categorical variables were tested using the Fisher's exact test or chi-square test. Differential analysis between groups of quantitative data were calculated using Wilcoxon rank-sum test. The receiver operating characteristic (ROC) curve was performed to calculate the area under the curve (AUC). For each model, the values of accuracy, precision, recall, F1 score, ROC curve and AUC value were conducted to evaluate the predictive ability of models. All statistical analysis were completed by R software (version 4.2.2, <https://cloud.r-project.org/>).

Construction of prediction model.

Those indicators which were redundant or with null values more than 10% were removed for model construction. 80% of the original data was taken as a training set, and the remaining 20% was taken as a test set. A hierarchical partitioning method is adopted to make the proportion of data of target subtypes (positive samples) and other subtypes (negative samples) in the training set and the test set consistent.

The training set and test set were both divided into four parts according to four molecular subtypes of breast cancer. Four prediction models were constructed based on each part of the training set and tested in each part of the test set. In addition, over the course of training on each molecular subtype, models used selected features of CUS, SWE, CEUS and full parameters were generated, respectively.

The predicting models in this study were constructed based on the combination of gradient boosting decision Tree frameworks and neural network frameworks on the model building and testing platform of AutoGluon (<https://auto.gluon.ai/stable/index.html>). To achieve great performance, AutoGluon is based on three main principles: (1) training a variety of different models, (2) using bagging when training those models, and (3) stack-ensembling those models to combine their predictive power into a "super" model. Bagging (Bootstrap Aggregation) is a technique used in machine learning to improve the stability and accuracy of algorithms. The key idea is that combining multiple models usually leads to better performance than any single model because it reduces overfitting and adds robustness to the prediction. AutoGluon performs bagging in a different way by combining it with

cross-validation. At prediction time, bagging takes all these individual models and averages their predictions to generate a final answer. Cross-validation allows us to train and validate multiple models using all the training data. The training data is partitioned into K folds or subsets of the dataset. Each model instance is evaluated against the hold-out fold that isn't used during training. The predictions then are concatenated from the folds to create the out-of-fold predictions. The final model cross-validation score was calculated by computing the evaluation metric using the out-of-fold predictions and the target ground truth. Stacked ensembling is a multi-layer model. Each layer consists of several different bagged models that use the predictions from the previous layer as features in addition to the original features from the training data. The first layer uses only the original features from the training data. The last layer consists of a single "super" model that combines the predictions from the second to last layer.

To make the new model have higher accuracy and better ROC curve, the variables were selected by importance of variable. Computed via permutation-shuffling, feature importance scores quantify the drop in predictive performance when one column's values are randomly shuffled across rows. Features with non-positive importance score hardly contribute to the predictor's accuracy, or may even be actively harmful to include in the data. These features are removed from the data. Based on the selected effective feature subset, binary prediction models of features of CUS, features of SWE, features of CEUS and full parameters were constructed separately for the four breast cancer subtypes Luminal A, Luminal B, HER2, and TNBC, respectively.

## Results

### Baseline characteristics

According to the inclusion and exclusion criteria, 157 patients were included in this study. The patients' clinical characteristics are summarized in Table 1. Based on molecular detection results, 48 patients were Luminal A subtype, 64 patients were Luminal B subtype, 27 patients were HER2 subtype, 18 patients were TNBC subtype. The median age was 51 years of all patients, 49.5 of Luminal A, 50 of Luminal B, 55 of HER2, 52.5 of TNBC and there was no significant difference between molecular subtypes. Postmenopausal patients were 79 (50%), 21 (44%), 30 (47%) and 18 (67%) in all patients, Luminal A, Luminal B, HER2 and TNBC, respectively. It was indicated that HER2 and TNBC tend to occur in older menopausal women.

Features of CUS, SWE and CEUS between molecular subtypes of breast cancer.

There were seven parameters which had significant difference between molecular subtypes in the examination

**Table 1** Clinical characteristic of molecular subtype groups

Characteristic	Overall (n = 157)	Luminal A (n = 48)	Luminal B (n = 64)	HER2 (n = 27)	TNBC (n = 18)
Age	51.00(45.00,58.00)	49.50(46.50,60.25)	50.00(43.00,59.00)	55.00(51.00,56.00)	52.50(45.75,57.50)
BMI	23.05(21.37,25.30)	23.10(21.42,26.39)	23.23(21.76,24.94)	22.19(20.11,24.56)	23.00(22.29,24.59)
Menopause	79 (50%)	21 (44%)	30 (47%)	18 (67%)	10 (56%)
Lymph node metastasis	45 (29%)	8 (17%)	22 (34%)	8 (30%)	7 (39%)
Her-2					
Negative	119 (76%)	48 (100%)	53 (83%)	0 (0%)	18 (100%)
Positive	38 (24%)	0 (0%)	11 (17%)	27 (100%)	0 (0%)
Ki-67					
Negative	55 (35%)	48 (100%)	4 (6.3%)	1 (3.7%)	2 (11%)
Positive	102 (65%)	0 (0%)	60 (94%)	26 (96%)	16 (89%)
ER					
Negative	45 (29%)	0 (0%)	0 (0%)	27 (100%)	18 (100%)
Positive	112 (71%)	48 (100%)	64 (100%)	0 (0%)	0 (0%)
PR					
Negative	64 (41%)	4 (8.3%)	15 (23%)	27 (100%)	18 (100%)
Positive	93 (59%)	44 (92%)	49 (77%)	0 (0%)	0 (0%)
Histologic grade					
I	17 (11%)	9 (19%)	8 (13%)	0 (0%)	0 (0%)
II	87 (55%)	28 (58%)	41 (64%)	12 (44%)	6 (33%)
III	28 (18%)	0 (0%)	12 (19%)	8 (30%)	8 (44%)
Differentiated degree					
Medium differentiated	87 (55%)	28 (58%)	41 (64%)	12 (44%)	6 (33%)
Low differentiated	27 (17%)	0 (0%)	11 (17%)	8 (30%)	8 (44%)
High differentiated	16 (10%)	9 (19%)	7 (11%)	0 (0%)	0 (0%)

result of CUS (Table 2). In BI-RADS, most patients in grade 4a were Luminal A (51.43%) and most patients of grade 4c and grade 5 were Luminal B (47.06%, 72.73%). Almost half of the patients who had palpable mass were Luminal B (44.12%). Patients with HER2 had lower aspect ratio (median: 0.6) and larger maximum diameter (median: 25 mm) than others. HER2 patients had a higher ratio of calcification (89%) and heterogeneous echogenicity (96%). The proportion of TNBC patients was the least in patients with calcification (9.64%), irregular shape (10.60%) and heterogeneous echogenicity (11.02%). In the examination result of SWE, the Esd was 13.27 of all patients, 14.65 of Luminal A, 12.10 of Luminal B, 16.10 of HER2, 10.97 of TNBC and different significantly (Table 3). There were two parameters which had significant difference between molecular subtypes in the examination result of CEUS (Table 4). The time of appearance was 9 s of all patients, 9 s of Luminal A, 8 s of Luminal B, 9 s of HER2, 8.5 s of TNBC. The PI was 26.99 db of all patients, 26.54 db of Luminal A, 25.75 db of Luminal B, 32.16 db of HER2, 29.25 db of TNBC. These differential features can enhance the classification ability of the model.

### Results of prediction models

The performance of prediction models validating on test set was shown in Table 5, and the ROC curves were shown in Fig. 1. In the test set of Luminal A, full

parameters model had highest model evaluation indicators except precision (accuracy = 0.81, precision = 0.80, recall = 0.81, F1 = 0.80, AUC = 0.81). In the test set of Luminal B, the full parameter model had better performance (accuracy = 0.74, precision = 0.74, recall = 0.73, F1 = 0.74, AUC = 0.74). The evaluation results of test set of TNBC were the same as results of Luminal B (accuracy = 0.87, precision = 0.80, recall = 0.87, F1 = 0.81, AUC = 0.78). On the HER2 test set, the SWE model had higher values of precision, recall and F1 score (accuracy = 0.78, precision = 0.77, recall = 0.79, F1 = 0.79, AUC = 0.84). However, full parameter models had the highest AUC values in every test set. In aggregate, judging from the values of accuracy, precision, recall, F1 score and AUC, models used features selected from full parameters showed better prediction results than those used features selected from CUS, SWE and CEUS alone.

### Discussion

The determination of breast cancer molecular subtypes primarily relies on clinical methods such as biopsy or postoperative pathological immunohistochemical assays. This study examined the correlation between multimodal ultrasound features and breast cancer molecular subtypes using SWE and CEUS, based on conventional two-dimensional ultrasound and CDFI. Furthermore, structural data of CUS, SWE and CEUS were combined to construct multimodal ultrasound models to predict

**Table 2** Characteristic of CUS of molecular subtype groups

Characteristic	Overall (n = 157)	Luminal A (n = 48)	Luminal B (n = 64)	HER2 (n = 27)	TNBC (n = 18)
BI-RADS					
3	2 (1.3%)	1 (2.1%)	1 (1.6%)	0 (0%)	0 (0%)
4a	35 (22%)	18 (38%)	11 (17%)	2 (7.4%)	4 (22%)
4b	75 (48%)	20 (42%)	28 (44%)	16 (59%)	11 (61%)
4c	34 (22%)	9 (19%)	16 (25%)	7 (26%)	2 (11%)
5	11 (7.0%)	0 (0%)	8 (13%)	2 (7.4%)	1 (5.6%)
Palpable mass	102 (65%)	25 (52%)	45 (70%)	22 (81%)	10 (56%)
Location					
Left	83 (53%)	29 (60%)	33 (52%)	15 (56%)	6 (33%)
Right	74 (47%)	19 (40%)	31 (48%)	12 (44%)	12 (67%)
Distance to nipple					
< 20 mm	89 (57%)	29 (60%)	33 (52%)	17 (63%)	10 (56%)
> 20 mm	68 (43%)	19 (40%)	31 (48%)	10 (37%)	8 (44%)
Maximum diameter	19.00(14.00,28.00)	17.00(11.75,24.25)	19.00(15.00,30.00)	25.00(18.50,35.00)	18.00(15.25,21.75)
Aspect ratio	0.73(0.58,0.86)	0.74(0.61,0.87)	0.75(0.64,0.87)	0.60(0.49,0.73)	0.70(0.61,0.86)
Blood flow signal					
0	15 (9.6%)	6 (13%)	6 (9.4%)	2 (7.4%)	1 (5.6%)
1	54 (34%)	18 (38%)	21 (33%)	7 (26%)	8 (44%)
2	58 (37%)	18 (38%)	25 (39%)	10 (37%)	5 (28%)
3	30 (19%)	6 (13%)	12 (19%)	8 (30%)	4 (22%)
Resistance index	0.80(0.72,1.00)	0.77(0.67,1.00)	0.82(0.71,1.00)	0.81(0.75,1.00)	1.00(0.76,1.00)
Calcification	103 (66%)	28 (58%)	41 (64%)	24 (89%)	10 (56%)
Margin					
Clear	75 (48%)	23 (48%)	32 (50%)	11 (41%)	9 (50%)
Unclear	82 (52%)	25 (52%)	32 (50%)	16 (59%)	9 (50%)
Shape					
Irregular	151 (96%)	46 (96%)	64 (100%)	25 (93%)	16 (89%)
Regular	6 (3.8%)	2 (4.2%)	0 (0%)	2 (7.4%)	2 (11%)
Echogenicity					
Heterogeneous	127 (81%)	34 (71%)	53 (83%)	26 (96%)	14 (78%)
Homogeneous	30 (19%)	14 (29%)	11 (17%)	1 (3.7%)	4 (22%)
Peripheral duct	60 (38%)	17 (35%)	24 (38%)	11 (41%)	8 (44%)
Posterior echo attenuation	21 (13%)	7 (15%)	7 (11%)	5 (19%)	2 (11%)

the molecular subtype of breast cancer. We found that the full parameter model achieved better results compared to the others and revealed the feasibility of multimodal ultrasound models in predicting molecular subtype of breast cancer, which have important guiding value for clinical diagnosis and treatment.

We observed significant differences in ten parameters across molecular subtypes of breast cancer, suggesting potential correlations with the phenotypic manifestations of these subtypes. Luminal A and Luminal B types of breast cancer usually have a lower degree of malignancy and primarily grow in an infiltrative manner. Therefore, when the lesions invade surrounding tissues such as lymphatic and blood vessels, spiculations, angular margins, or ill-defined edges may be displayed on ultrasound images. However, since the incidence rates of Luminal A and Luminal B types are relatively higher compared to the other two types, they account for a higher proportion in each category of the BI-RADS classification.

Patients with HER2 tumors tended to have a higher degree of malignancy and faster growth and exhibited lower aspect ratios, larger maximum diameters, higher calcification rates and greater echogenicity heterogeneity. Given the close relationship between the Her-2 gene and angiogenesis, as well as the expression of vascular endothelial growth factor (VEGF), which promotes endothelial cell proliferation, tumor growth, invasion and metastasis, necrosis is more likely to occur within these tumors [20]. They are more likely to experience local tissue necrosis and subsequent calcification. These findings align with the research conducted by Magdale et al. [21], who further noted that posterior acoustic enhancement was more prevalent in aggressive cancers (Luminal B, HER2 and TNBC) and associated with a higher tumor cell count and a tendency towards high-grade tumors [22]. Conversely, TNBC patients demonstrated the lowest proportions of calcification, irregular shape, and echogenicity heterogeneity, like those of benign masses.

**Table 3** Characteristic of SWE of molecular subtype groups

Characteristic	Overall (n = 157)	Luminal A (n = 48)	Luminal B (n = 64)	HER2 (n = 27)	TNBC (n = 18)
SWE grade					
I	3 (2%)	2 (4%)	0 (0%)	1 (4%)	0 (0%)
II	26 (16%)	9 (19%)	12 (19%)	1 (4%)	4 (22%)
III	85 (54%)	28 (58%)	36 (56%)	13 (48%)	7 (39%)
IV	44 (28%)	9 (19%)	16 (25%)	12 (44%)	7 (39%)
Hard edge sign	127 (81%)	38 (79%)	51 (80%)	25 (93%)	13 (72%)
Emean	43.93 (35.27,50.99)	40.85 (34.31,49.77)	43.87 (34.83,50.11)	45.94 (40.19,54.47)	43.64 (35.54,46.22)
E <sub>max</sub>	101.37 (78.37,138.37)	99.07 (80.46,129.73)	103.47 (77.85,144.62)	127.50 (91.51,151.02)	93.27 (73.88,110.74)
E <sub>min</sub>	15.56 (10.31,22.51)	13.99 (8.78,19.76)	16.07 (10.69,22.24)	19.17 (10.34,23.83)	18.09 (12.51,24.77)
E <sub>sd</sub>	13.27 (9.84,18.38)	14.65 (11.57,19.08)	12.10 (9.18,15.50)	16.10 (13.54,19.35)	10.97 (8.57,14.20)
E <sub>smean</sub>	49.48 (40.84,56.19)	47.58 (37.46,56.91)	49.93 (44.10,55.85)	49.85 (43.70,56.11)	45.40 (40.02,54.07)
E <sub>smax</sub>	127.51 (101.46,164.74)	119.70 (94.73,154.39)	135.96 (103.69,165.44)	137.32 (121.80,165.19)	107.89 (96.91,136.48)
E <sub>smin</sub>	13.44 (6.44,18.89)	12.52 (6.18,18.03)	15.46 (7.48,19.71)	12.24 (5.20,18.51)	15.71 (7.73,18.74)
E <sub>ssd</sub>	18.94 (14.87,24.92)	19.17 (13.09,25.68)	18.81 (14.97,25.17)	21.31 (17.67,23.35)	16.33 (13.57,19.01)
E <sub>lsmean</sub>	46.54 (38.32,53.81)	45.42 (36.29,54.69)	46.71 (39.15,53.35)	47.18 (43.56,55.02)	44.39 (37.04,48.65)
E <sub>lsmax</sub>	133.63 (105.55,167.53)	119.70 (98.90,154.39)	138.39 (106.07,171.16)	147.30 (124.16,165.46)	111.46 (98.03,136.48)
E <sub>lsmin</sub>	12.24 (6.29,18.70)	11.08 (6.18,15.22)	12.99 (7.07,19.37)	11.34 (5.20,18.28)	13.46 (7.73,18.74)
E <sub>lssd</sub>	17.01 (13.10,21.43)	17.74 (12.82,23.05)	15.20 (13.06,21.28)	19.04 (16.24,22.52)	14.51 (12.71,18.27)

Abbreviation: Emean, Mean elastic modulus value of lesion; E<sub>max</sub>, Maximum elastic modulus value of lesion; E<sub>min</sub>, Minimum elastic modulus value of lesion; E<sub>sd</sub>, Standard deviation elastic modulus value of lesion; E<sub>smean</sub>, Mean elastic modulus value of shell; E<sub>smax</sub>, Maximum elastic modulus value of shell; E<sub>smin</sub>, Minimum elastic modulus value of shell; E<sub>ssd</sub>, Standard deviation elastic modulus value of shell; E<sub>lsmean</sub>, Mean elastic modulus value of both lesion and shell; E<sub>lsmax</sub>, Maximum elastic modulus value of both lesion and shell; E<sub>lsmin</sub>, Minimum elastic modulus value of both lesion and shell; E<sub>lssd</sub>, Standard deviation elastic modulus value of both lesion and shell

Zhang et al. described this subtype using two distinct American image patterns: one characterized by irregular shape, lobular margins, lack of calcification and vessels, and the other featuring oval shapes, lobular margins, and an absence of visible vessels [23]. TNBC typically exhibits high histological grades and Ki-67 levels, often presenting on ultrasound with micro-lobulated margins and minimal blood flow. Distinct from other subtypes, TNBC tends to follow a specific growth pattern of rapid proliferation, with tumor cells pushing against the margins and minimal connective tissue reaction, resulting in well-defined micro-lobulated edges [24]. Because the tumor grows rapidly, the central part is prone to necrosis, resulting in fewer overall blood flow signals.

In the results of SWE examinations, statistically significant differences were observed in the E<sub>sd</sub> among the molecular subtypes. Specifically, the Luminal A subtype had the highest E<sub>sd</sub>, with a value of 14.65, while the TNBC subtype had the lowest, at 10.97. A high Ki-67 proliferation index is commonly seen in Luminal B, HER2 overexpression, and TNBC subtypes, while Luminal A subtype usually has a lower Ki-67 proliferation index. This may be related to the fact that a high Ki-67 proliferation index indicates more active and rapidly growing tumor cells, which continuously adhere to and invade the extracellular matrix, causing the mass to adhere to the surrounding tissue and increase in hardness. These findings are consistent with the research conducted by Hyunjin Kim et al., who reported that the Ki-67 positive

E<sub>sd</sub> was significantly higher than that of Ki-67 negative lesions. Additionally, they found that the Ki-67 positive E<sub>max</sub> and E<sub>sd</sub> were higher than those of Ki-67 negative lesions, although these differences were not statistically significant [25].

CEUS is a pure blood pool imaging technique that can reflect the perfusion information of blood flow within lesions, enhancing the contrast between blood and surrounding tissues, and thereby improving the signal-to-noise ratio of CEUS images. In recent years, it has been widely used in the differential diagnosis of benign and malignant breast lesions and the evaluation of the effects of neoadjuvant chemotherapy for breast cancer [26]. In this study, there were statistically significant differences in the enhancement time and PI among the four types of breast cancer, which is related to the formation of arteriovenous fistulas and thrombosis in vessels within malignant lesions. Breast cancer is a vasculature-dependent disease, and the differences in CEUS enhancement patterns between breast cancer lesions and surrounding normal breast tissues are closely related to their blood perfusion and pathological characteristics. Breast cancers with higher histological grades tend to have poorer differentiation, higher malignancy, and increased angiogenesis. Positive expression of ER and/or PR indicates that cancer cell growth and proliferation are still regulated by endocrine factors [27]. Higher levels of positive ER and/or PR expression suggest better tumor differentiation, fewer pathological vascular formations, and

**Table 4** Characteristic of CEUS of molecular subtype groups

Charac- teristic	Overall (n = 157)	Luminal A (n = 48)	Luminal B (n = 64)	HER2 (n = 27)	TNBC (n = 18)
Time of appearance	9.00(7.00,10.00)	9.00(8.00,11.00)	8.00(7.00,9.75)	9.00(7.50,10.50)	8.50(7.00,9.00)
Time of peak	15.00(13.00,18.00)	16.00(14.00,18.00)	15.00(13.00,17.00)	16.00(14.00,18.50)	15.00(13.25,16.75)
Time from appearance to peak	7.00(6.00,8.00)	6.00(5.25,8.00)	7.00(6.00,8.00)	7.00(6.00,8.00)	7.00(6.00,8.75)
Time of fading	40.00(34.00,49.00)	37.00(31.25,47.75)	40.50(34.25,51.75)	40.00(37.50,47.50)	36.00(30.25,47.25)
Enhancement border					
Clear	64 (41%)	16 (33%)	28 (44%)	15 (56%)	5 (28%)
Un-clear	93 (59%)	32 (67%)	36 (56%)	12 (44%)	13 (72%)
Enhancement pattern					
Irregular	133 (85%)	41 (85%)	55 (86%)	21 (78%)	16 (89%)
Regular	24 (15%)	7 (15%)	9 (14%)	6 (22%)	2 (11%)
Enhancement distribution					
Heterogeneous	118 (75%)	32 (67%)	49 (77%)	22 (81%)	15 (83%)
Homogeneous	38 (24%)	16 (33%)	14 (22%)	5 (19%)	3 (17%)
Enhancement intensity					
High	138 (88%)	40 (83%)	56 (88%)	24 (89%)	18 (100%)
Low	2 (1.3%)	1 (2.1%)	1 (1.6%)	0 (0%)	0 (0%)
None	4 (2.5%)	2 (4.2%)	2 (3.1%)	0 (0%)	0 (0%)
Normal	13 (8.3%)	5 (10%)	5 (7.8%)	3 (11%)	0 (0%)
Enhancement direction					
Centrifugal	15 (9.6%)	6 (13%)	6 (9.4%)	2 (7.4%)	1 (5.6%)
Centripetal	116 (74%)	35 (73%)	47 (73%)	19 (70%)	15 (83%)
Diffuse	22 (14%)	5 (10%)	9 (14%)	6 (22%)	2 (11%)

**Table 4** (continued)

Charac- teristic	Overall (n = 157)	Luminal A (n = 48)	Luminal B (n = 64)	HER2 (n = 27)	TNBC (n = 18)
Perfu- sion defects	77 (49%)	23 (48%)	33 (52%)	10 (37%)	11 (61%)
Crab- claw- like pattern	62 (39%)	18 (38%)	25 (39%)	12 (44%)	7 (39%)
En- hance- ment area					
Equal	34 (22%)	12 (25%)	14 (22%)	6 (22%)	2 (11%)
Larger	123 (78%)	36 (75%)	50 (78%)	21 (78%)	16 (89%)
En- hance- ment time					
De- layed	11 (7.0%)	4 (8.3%)	6 (9.4%)	0 (0%)	1 (5.6%)
Early	88 (56%)	28 (58%)	33 (52%)	17 (63%)	10 (56%)
Syn- chro- nous	58 (37%)	16 (33%)	25 (39%)	10 (37%)	7 (39%)
Rapid en- hance- ment	122 (78%)	40 (83%)	47 (73%)	21 (78%)	14 (78%)
Rapid fading	80 (51%)	29 (60%)	31 (48%)	14 (52%)	6 (33%)
BI	2.16(0.99,3.49)	2.01(0.95,3.57)	2.01(1.00,3.24)	2.64(1.00,5.58)	2.46(1.21,5.35)
AT	8.28(6.50,9.80)	8.33(7.29,10.26)	7.91(6.20,9.65)	8.50(7.68,9.87)	7.80(6.78,9.52)
TTP	16.50(13.51,20.01)	16.65(13.50,22.42)	16.50(13.62,19.75)	16.56(13.93,19.83)	14.93(12.80,17.78)
PI	26.99(21.83,32.76)	26.54(21.47,30.64)	25.75(19.94,30.53)	32.16(24.46,35.77)	29.25(25.04,33.13)
AS	0.65(0.52,0.84)	0.63(0.49,0.89)	0.66(0.53,0.83)	0.65(0.49,0.79)	0.71(0.58,0.83)
DT/2	91.91(75.60,115.03)	85.65(66.35,104.77)	93.60(78.80,118.00)	107.30(88.40,122.75)	80.36(75.62,105.23)
DS	-0.13(-0.18,-0.10)	-0.14(-0.20,-0.11)	-0.13(-0.18,-0.10)	-0.12(-0.17,-0.10)	-0.15(-0.17,-0.11)
AUTIC	1,680.37(1,102.60,2,131.93)	1,535.61(1,063.06,1,956.72)	1,569.23(1,058.75,2,056.55)	1,912.24(1,548.84,2,268.58)	1,641.23(1,295.87,2,114.50)
MTT	85.80(67.78,105.34)	80.37(60.26,99.40)	86.10(69.30,106.12)	97.15(77.30,114.66)	70.84(68.45,98.35)

Abbreviation: BI, Basic intensity; AT, Arrive time; TTP, Time to peak; PI, Peak intensity; AS, Ascent slope; DT/2, Descending time 2; DS, Descending slope; AUTIC, Area under time intensity curve; MTT, Mean transit time

slower contrast agent inflow. Her-2 positive expression is associated with increased vascular formation within breast lesions, and Her-2 expression positively correlates with high expression of vascular endothelial growth factor (VEGF), which promotes tumor vascular formation, therefore, high Her-2 expression reflects a high proliferative state of tumor cells. TNBC, which lacks expression of ER, PR, and Her-2, has the worst prognosis and shortest disease-free survival. The CEUS enhancement pattern of this subtype often appears as a clearly defined boundary, similar to that of benign tumors, which could be easily overlooked [28].

Our study has several limitations. Firstly, when analyzing the CEUS enhancement patterns and perfusion

parameters, we selected the most irregular or the most vascularized slice, which may not reflect the overall blood flow perfusion status of the tumor. Secondly, except for the quantitative analysis of CEUS, the remaining parameters were manually identified. Although all examinations were conducted by experienced sonographers, the subjectivity could not be eliminated from influencing the results. Thirdly, the inclusion of a relatively small sample of HER2 and TNBC patients may impact on certain statistical outcomes. Fourthly, due to the small sample size of this study, some samples with a small amount of missing data were included, therefore, the important variables identified through research and comparison may not be comprehensive enough. And, we constructed separate

**Table 5** Results of models in predicting molecular subtype of BRCA

Models	Accuracy	Precision	Recall	F1	AUC
Luminal A					
Full Parameter	0.81	0.80	0.81	0.80	0.81
CUS	0.74	0.81	0.74	0.66	0.74
SWE	0.74	0.73	0.74	0.73	0.79
CEUS	0.77	0.77	0.77	0.74	0.77
Luminal B					
Full Parameter	0.74	0.74	0.73	0.74	0.74
CUS	0.71	0.72	0.71	0.72	0.72
SWE	0.68	0.67	0.68	0.67	0.73
CEUS	0.71	0.74	0.71	0.68	0.71
HER2					
Full Parameter	0.81	0.77	0.79	0.78	0.89
CUS	0.75	0.74	0.76	0.75	0.87
SWE	0.78	0.77	0.79	0.79	0.84
CEUS	0.76	0.76	0.77	0.77	0.76
TNBC					
Full Parameter	0.87	0.80	0.87	0.81	0.78
CUS	0.87	0.77	0.87	0.81	0.75
SWE	0.87	0.76	0.87	0.81	0.74
CEUS	0.81	0.75	0.81	0.78	0.70

prediction models for each molecular subtype rather than a single model with molecular subtype as a combined outcome variable. While a unified model could provide an overview of predictor-subtype associations, we opted for subtype-specific models to better capture the unique biological and clinical characteristics of each subtype. This approach enhances interpretability and aligns with clinical decision-making, where subtype-specific insights are often required. However, we acknowledge that a combined model could offer additional perspectives and encourage future studies to explore this approach to further refine predictive frameworks in this field.

We will try to conduct multicenter studies in the future, leveraging a larger sample size and radiomics based on American imaging standards, which aims to develop a more robust model to validate the findings of our current study. Furthermore, we hope that the results can be applied to clinical practice, offering benefits to patients.

## Conclusion

In conclusion, multimodal ultrasound features had differences between molecular subtypes of breast cancer and models based on multimodal ultrasound data facilitated the prediction of molecular subtypes.

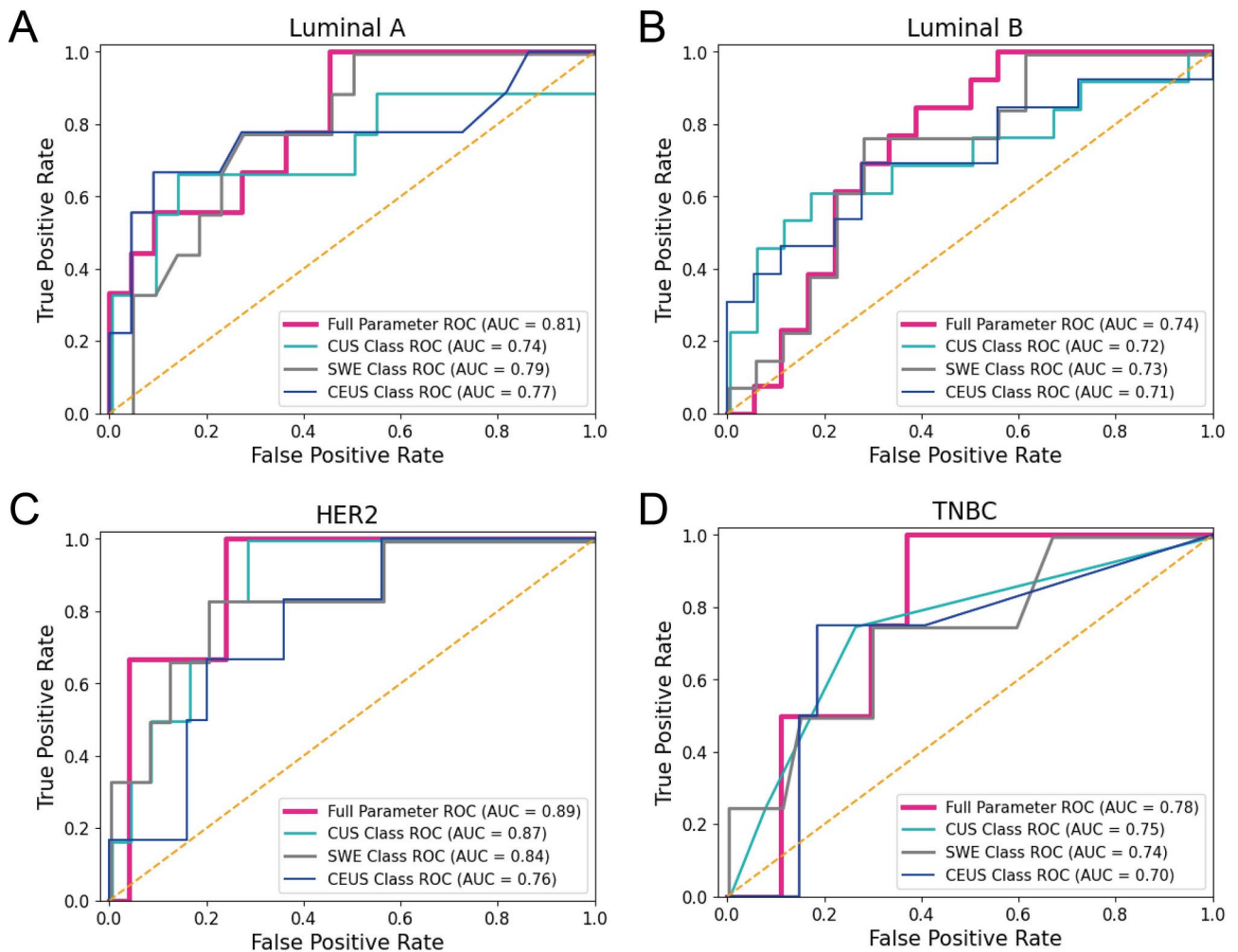


**Fig. 1** ROC curves of each model predicting test set of (A) Luminal A, (B) Luminal B, (C) HER2, (D) TNBC

**Abbreviations**

- AUC area under the curve
- CDFI color doppler flow imaging
- CEUS contrast-enhanced ultrasound
- CUS conventional ultrasound
- ER estrogen receptor
- Her-2 human epidermal growth factor receptor 2
- HER2 HER2-overexpressing
- PR progesterone receptor
- ROC receiver operating characteristic
- TNBC triple-negative breast cancer
- SWE shear wave elastography

**Acknowledgements**

The authors appreciate all patients and colleagues who participated in this study.

**Author contributions**

Author Contributions Conceptualization, H.L. and SH.X; Formal analysis, CT.Z. and HG.S.; Funding acquisition, H.L. and SH.X; Investigation, CT.Z. and HG.S.; Methodology, CT.Z.; Project administration, H.L. and SH.X; Resources, H.L.; Validation, CT.Z. and HG.S.; Visualization, CT.Z. and HG.S.; Writing - original draft, M.W., L.P., H.L. and HG.S.; Writing - review & editing, ZY.L., L.P., H.L., HG.S., CT.Z. and SH.X.

**Funding**

This study was funded by the Wenzhou Municipal Science and Technology Plan Project (Project Number: Y20220451), the Key Research and Development Program of Zhejiang Province (Project Number: 2021C03003) and the Basic Scientific Research Project of Wenzhou (Project Number: Y20240967).

**Data availability**

The data supporting the conclusions of this article will be made available from the corresponding author on reasonable request.

**Declarations**

**Ethical approval and consent to participate**

The studies involving humans were approved by the Ethics Committee in Clinical Research (ECCR) of the First Affiliated Hospital of Wenzhou Medical University (No. KY2022-R169). The studies were conducted in accordance with the local legislation and institutional requirements. All donors provided written informed consent

**Consent for publication**

Not applicable.

**Competing interests**

The authors declare no competing interests.

**Clinical trial number**

Chinese Clinical Trial Registry (No. ChiCTR2400082262).

**Author details**

<sup>1</sup>New District of the First Affiliated Hospital of Wenzhou Medical University, Shang-cai Village, Nan-bai-xiang Street, Ou-hai District, Wenzhou City 325000, Zhejiang Province, China

<sup>2</sup>School of advanced manufacturing/school of ocean, Fuzhou University, No.1 Shui-cheng Road, Jin-jing Town, Jin-jiang City 362251, Fujian Province, China

<sup>3</sup>Institute of Hepatology and Epidemiology, Hangzhou Xixi Hospital, Zhejiang Chinese Medical University, 2 Heng-bu Street, Xi-hu District, Hangzhou City 310023, Zhejiang Province, China

<sup>4</sup>Department of Ultrasound, Hangzhou Xixi Hospital Affiliated to Zhejiang Chinese Medical University, 2 Heng-bu Street, Xi-hu District, Hangzhou City 310023, Zhejiang Province, China

<sup>5</sup>Department of Graduate, Wenzhou Medical University, Cha-shan Street Higher Education Park, Ou-hai District, Wenzhou City 325035, Zhejiang Province, China

Received: 6 September 2024 / Accepted: 28 April 2025

Published online: 19 May 2025

**References**

- Siegel RL, Miller KD, Wagle NS, Jemal A. Cancer statistics, 2023. *CA Cancer J Clin.* 2023;73(1):17–48.
- Xia C, Dong X, Li H, et al. Cancer statistics in China and united States, 2022: profiles, trends, and determinants. *Chin Med J (Engl).* 2022;135(5):584–90.
- Barzgar Barough N, Sajjadi F, Jalilzadeh N, Shafaei H, Velaei K. Understanding breast cancer heterogeneity through non-genetic heterogeneity. *Breast Cancer.* 2021;28(4):777–91.
- Ding K, Chen F, Priedigkeit N, et al. Single cell heterogeneity and evolution of breast cancer bone metastasis and organoids reveals therapeutic targets for precision medicine. *Ann Oncol.* 2022;33(10):1085–8.
- Goldhirsch A, Wood WC, Coates AS, et al. Strategies for subtypes—dealing with the diversity of breast cancer: highlights of the St. Gallen international expert consensus on the primary therapy of early breast Cancer 2011. *Ann Oncol.* 2011;22(8):1736–47.
- Lalani N, Voduc KD, Jimenez RB, et al. Breast Cancer molecular subtype as a predictor of radiation therapy fractionation sensitivity. *Int J Radiat Oncol Biol Phys.* 2021;109(1):281–7.
- Ji Y, Whitney HM, Li H, et al. Differences in molecular subtype reference standards impact AI-based breast Cancer classification with dynamic Contrast-enhanced MRI. *Radiology.* 2023;307(1):e220984.
- Berg WA, Bandos AI, Mendelson EB et al. Ultrasound as the primary screening test for breast cancer: analysis from ACRIN 6666. *J Natl Cancer Inst.* 2016;108(4).
- Niell BL, Freer PE, Weinfurter RJ, Arleo EK, Drukteinis JS. Screening for breast Cancer. *Radiol Clin North Am.* 2017;55(6):1145–62.
- Banys-Paluchowski M, Rubio IT, Karadeniz Cakmak G, et al. Intraoperative Ultrasound-Guided excision of Non-Palpable and palpable breast cancer: systematic review and Meta-Analysis. *Ultraschall Med.* 2022;43(4):367–79.
- Wan C, Zhou L, Li H et al. Multiparametric Contrast-Enhanced ultrasound in early prediction of response to neoadjuvant chemotherapy and Recurrence-Free survival in breast Cancer. *Diagnostics (Basel).* 2023;13(14).
- Li X, Zhang J, Zhang G, et al. Contrast-Enhanced ultrasound and conventional ultrasound characteristics of breast Cancer with different molecular subtypes. *Clin Breast Cancer.* 2024;24(3):204–14.
- Carlsen J, Ewertsen C, Sletting S, et al. Ultrasound elastography in breast Cancer diagnosis. *Ultraschall Med.* 2015;36(6):550–62. quiz 563–555.
- Sultan LR, Schultz SM, Cary TW, Sehgal CM. Machine learning to improve breast cancer diagnosis by multimodal ultrasound. *IEEE Int Ultrason Symp.* 2018;2018.
- Gu J, Zhong X, Fang C, et al. Deep learning of multimodal ultrasound: stratifying the response to neoadjuvant chemotherapy in breast Cancer before treatment. *Oncologist.* 2024;29(2):e187–97.
- Cai L, Sidey-Gibbons C, Nees J, et al. Can multi-modal radiomics using pre-treatment ultrasound and tomosynthesis predict response to neoadjuvant systemic treatment in breast cancer? *Eur Radiol.* 2024;34(4):2560–73.
- Curigliano G, Burstein HJ, Winer EP, et al. De-escalating and escalating treatments for early-stage breast cancer: the St. Gallen international expert consensus conference on the primary therapy of early breast Cancer 2017. *Ann Oncol.* 2017;28(8):1700–12.
- Adler DD, Carson PL, Rubin JM, Quinn-Reid D. Doppler ultrasound color flow imaging in the study of breast cancer: preliminary findings. *Ultrasound Med Biol.* 1990;16(6):553–9.
- Spak DA, Plaxco JS, Santiago L, Dryden MJ, Dogan BE. BI-RADS((R)) fifth edition: A summary of changes. *Diagn Interv Imaging.* 2017;98(3):179–90.
- Hasan R, Bhatt D, Khan S, et al. Association of Her-2 expression and clinicopathological parameters in colorectal carcinoma in Indian population. *Open Access Maced J Med Sci.* 2019;7(1):6–11.
- Gumowska M, Maczewska J, Prostko P, Roszkowska-Purska K, Dobruch-Sobczak K. Is there a correlation between multiparametric assessment in ultrasound and intrinsic subtype of breast cancer?? *J Clin Med.* 2021;10(22).
- Li JW, Zhang K, Shi ZT, et al. Triple-negative invasive breast carcinoma: the association between the sonographic appearances with clinicopathological feature. *Sci Rep.* 2018;8(1):9040.
- Zhang L, Li J, Xiao Y, et al. Identifying ultrasound and clinical features of breast cancer molecular subtypes by ensemble decision. *Sci Rep.* 2015;5:11085.
- Wang D, Zhu K, Tian J, et al. Clinicopathological and ultrasonic features of Triple-Negative breast cancers: A comparison with hormone Receptor-Positive/Human epidermal growth factor Receptor-2-Negative breast cancers. *Ultrasound Med Biol.* 2018;44(5):1124–32.
- Kim H, Lee J, Kang BJ, Kim SH. What shear wave elastography parameter best differentiates breast cancer and predicts its histologic aggressiveness? *Ultrasonography.* 2021;40(2):265–73.
- Huang Y, Le J, Miao A, et al. Prediction of treatment responses to neoadjuvant chemotherapy in breast cancer using contrast-enhanced ultrasound. *Gland Surg.* 2021;10(4):1280–90.
- Kalinina T, Kononchuk V, Alekseenok E et al. Expression of Estrogen Receptor- and progesterone Receptor-Regulating MicroRNAs in breast Cancer. *Genes (Basel).* 2021;12(4).
- Liang X, Li Z, Zhang L, Wang D, Tian J. Application of Contrast-Enhanced ultrasound in the differential diagnosis of different molecular subtypes of breast Cancer. *Ultrason Imaging.* 2020;42(6):261–70.

**Publisher's note**

Springer Nature remains neutral with regard to jurisdictional claims in published maps and institutional affiliations.